Extragalactic Jets: Theory and Observation from Radio to Gamma Ray
*ASP Conference Series, Vol. **VOLUME**, **YEAR OF PUBLICATION***
T. A. Rector and D. S. De Young (eds.)

Magnetic Field Structure in the Parsec Scale Jet of 3C 273 from Multifrequency VLBA Observations

T. Savolainen,[1,2] K. Wiik,[2] E. Valtaoja,[2] and M. Tornikoski[3]

[1] *Max-Planck-Institut für Radioastronomie, Auf dem Hügel 69, D-53121 Bonn, Germany*

[2] *Tuorla Observatory, University of Turku, Väisäläntie 20, FI-21500 Piikkiö, Finland*

[3] *Metsähovi Radio Observatory, Helsinki University of Technology, Metsähovintie 114, FI-02540 Kylmälä, Finland*

Abstract. We present first results from a multifrequency VLBA observations of 3C 273 in 2003. The source was observed simultaneously at 5.0, 8.4, 15.3, 22.2, 43.2 and 86.2 GHz, and from this multifrequency data set, spectra of 16 emission features in the parsec scale jet were carefully constructed by using a new model-fitting based method. The measured spectra and sizes of the emission features were used to calculate the magnetic field density and the energy density of the relativistic electrons in the different parts of the parsec scale jet, independent of any equipartition assumption. We measure magnetic field density of an order of 1 Gauss in the core. The magnetic energy density in the core dominates over that of the relativistic electrons, while in the downstream region our data are roughly consistent with an equipartition. A strong gradient in the magnetic field density across the jet width, coincident with a transverse velocity structure at about 1.5 mas from the core, was found: the slower superluminal component B2 on the northern side of the jet has a magnetic field density two orders of magnitude lower than the faster southern components B3 and B4.

1. Introduction

For over 30 years, Very Long Baseline Interferometry (VLBI) has been the prime observational method for studying compact extragalactic jets and it has been used extensively to investigate the morphology, kinematics, and polarization of the jets in parsec scales (see e.g. Zensus 1997). However, studies of the jets' continuum spectrum in the VLBI scale have been hitherto surprisingly rare, even though the synchrotron spectrum provides one of the very few available probes of the magnetic field and particle energy density in the jet (Marscher 1987). Pioneering observations of the jet spectrum in parsec scales were done in the 1980s (Cotton et al. 1980; Bartel et al. 1984; Marscher & Broderick 1985; Marscher 1988), but before the advent of the Very Long Baseline Array in 1993, it was not usually possible to observe the source simultaneously at several frequencies, and the typical flux density variability of the compact jets made it difficult to combine observations from different epochs. VLBA's frequency agility allows nowadays practically simultaneous multifrequency observations with a wide frequency coverage, and this has made the studies of the continuum spectrum of

the parsec scale jets feasible (see Lobanov 1998; Walker et al. 2000; Marr et al. 2001; Vermeulen et al. 2003; Savolainen 2006). However, due to tricky image alignment and uneven (u, v) plane coverage between different frequencies, extraction of the continuum spectra from a multifrequency VLBI data set is still a non-trivial task and requires a very careful planning, execution and analysis of the experiment. Only a very small number of sources have been studied so far.

In the present paper, we report the first results from the spectral analysis of multifrequency VLBA observations of the quasar 3C 273 ($z = 0.158$). In Section 2, we briefly describe our new method for extracting spectra of individual emission features in the jet from a multifrequency VLBI data set. In Section 3, the spectra observed on February 28, 2003 are presented, and the measured synchrotron turnover frequencies and flux densities are used to estimate the physical conditions in the jet, i.e. the magnetic field and the relativistic electron energy density. The results are discussed in Section 4.

Throughout the paper, we use a cosmology with $H_0 = 71$ km s^{-1} Mpc^{-1}, $\Omega_M = 0.27$, and $\Omega_\Lambda = 0.73$. This corresponds to a linear scale of 2.7 pc mas^{-1} for 3C 273. For the spectral index α, we use the positive convention: $S_\nu \propto \nu^{+\alpha}$.

2. Extraction of the spectra from multifrequency VLBI data

In the year 2003, 3C 273 was the target of a multiwavelength campaign organized to support the observations done with the INTEGRAL γ-ray satellite (Courvoisier et al. 2003). To complement this campaign with imaging data, we carried out a polarimetric multifrequency monitoring of 3C 273 using the VLBA. These observations are described in Savolainen et al. (2006, hereafter Paper I), where a kinematical analysis of the component motions was presented. 3C 273 was observed with the VLBA five times in 2003 for nine hours at each epoch. Observations were made at six frequencies (5.0, 8.4, 15.3, 22.2, 43.2 and 86.2 GHz) and individual scans at different frequencies were interleaved in order to obtain practically simultaneous multifrequency data set. The calibration, imaging and self-calibration of the data were done by the standard procedures.

In the data reduction, special attention was paid to the amplitude calibration. The accuracy of the final flux density scale was checked by comparing the extrapolated zero baseline flux density of the compact calibrator source 3C 279 at 5, 8, 22 and 43 GHz, to the interpolated flux densities from the VLA polarization monitoring program (Taylor & Myers 2000), and at 86 GHz to the quasi-simultaneous data from the SEST telescope. The accuracy turned out to be as good as $\sim 5\%$ at the frequencies from 5 to 43 GHz and $\sim 20\%$ at 86 GHz.

Because the VLBI networks are not reconfigurable like, for example, the VLA, their (u, v) plane coverage differs significantly at different observing frequencies. Typically, in the spectral analysis of the multifrequency VLBI data, the (u, v) coverages at different frequencies have been matched either by simply throwing away the data at the large (u, v) radii at high frequencies or by tapering the data to a common (low) resolution. This has the consequence that a significant amount of data are not used and much of the attainable angular resolution is lost. A broad frequency coverage, which is needed to reliably measure the turnover of the synchrotron spectrum, exacerbates the problem: for a frequency coverage of $5 - 86$ GHz at the VLBA, the common range of (u, v) dis-

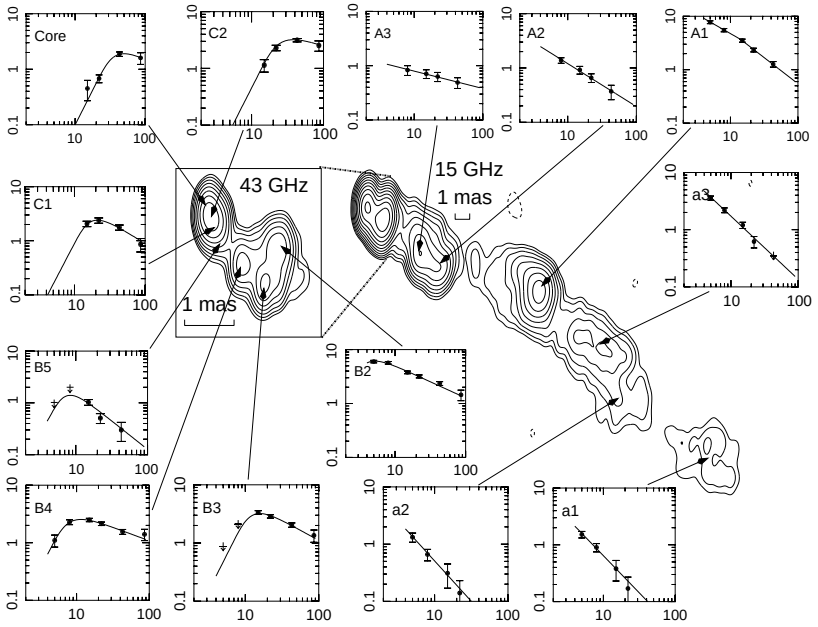

Figure 1. The radio spectra of the emission features in the parsec scale jet of 3C 273 observed on Feb 28, 2003. The figure also shows jet images at 15 and 43 GHz. In the spectral plots, the x-axis is frequency in GHz and the y-axis is flux density in Jy. The solid lines show either a power-law or a self-absorbed synchrotron spectrum fitted to the data. Downward arrows represent upper limits. Spectra of three weak components (B1, a4, a5) are omitted from the figure due to lack of space.

tances between the frequencies is only 4% of the whole range of observed (u, v) radii.

By using a model-fitting based spectral extraction method, the above-described problem with an uneven (u, v) coverage can be significantly relieved. The idea is to use *a priori* knowledge of the source structure, measured at high frequencies, to allow at lower frequencies the derivation of sizes and flux densities of even those emission features that have mutual separations less than the Rayleigh limit at the given frequency. This is possible because, if we have a template of the brightness distribution, the minimum resolvable size is a function of the signal-to-noise ratio of the visibility data, and for high SNR data, it can be much smaller than the Rayleigh limit (see e.g. Kovalev et al. 2005). In practice, this was done in the following way:

1) A simple source model, consisting of two-dimensional Gaussian components, was formed at 43 GHz. (In our case, since there were only 6 working antennas at 86 GHz, the best angular resolution was obtained at 43 GHz.)

2) This template model was transferred to 22 and 86 GHz. The relative positions of the components were fixed to the values obtained from model-fitting at 43 GHz, and the models were aligned by assuming that optically thin components have frequency independent positions.

3) Model-fitting was run at each frequency letting only component sizes and flux densities in the transferred model to vary. If any two components had a

Table 1. Fitted spectral and size parameters for inner jet components

Comp.	z_0 (mas)	$S_{\rm m}$ (Jy)	$\nu_{\rm m}$ (GHz)	α	$a(\nu_{\rm m})$ (mas)	δ
Core	0.00	1.9 ± 0.2	50 ± 10	-0.6 ± 0.4	0.07 ± 0.01	–
C2	0.15	3.2 ± 0.1	38 ± 1	-0.4 ± 0.1	0.09 ± 0.02	5.5 ± 1.9
C1	0.30	2.4 ± 0.2	21 ± 1	-0.8 ± 0.2	0.10 ± 0.03	–
B5	0.54	1.4 ± 0.2	8 ± 1	-1.1 ± 0.3	≈ 0.16	–
B4	1.07	2.5 ± 0.1	11.5 ± 0.6	-0.5 ± 0.1	0.22 ± 0.03	8.6 ± 3.2
B2	1.31	6.1 ± 0.3	5.2 ± 0.7	-0.6 ± 0.1	0.28 ± 0.06	7.1 ± 2.5
B3	1.54	3.2 ± 0.1	15.8 ± 0.7	-0.7 ± 0.1	0.23 ± 0.03	4.2 ± 1.7
B1	1.66	0.6 ± 0.2	11 ± 5	-0.2 ± 0.2	0.10 ± 0.03	–

separation smaller than $\sim 1/5$ of the beam size at the given frequency, these were replaced by single component in order not to try to extrapolate beyond (u, v) radius corresponding to $\sim 1/5$ of the beam size, which is the typical uncertainty of a component position (see Paper I). If the residual map contained significant emission that was not accounted for by the transfered model, a new model component(s) was added and model-fitting was run again. This produced a template model for the next lower frequency and steps 2 and 3 were repeated for all the frequencies.

4) We assume that the angular size of a component varies smoothly over the frequencies. The sizes of the components were inspected as a function of frequency, and fitted with a power-law after removing clear outliers. The results indicated that sizes are nearly constant or decreasing slowly as a function of frequency (the power-law indeces range from -0.3 to +0.1 with typical uncertainties of $0.1 - 0.2$).

5) The angular sizes of the components were fixed to the values derived from the power-law fit (typically a constant), and the model-fit was run again at all frequencies with the component flux densities as the only free parameters. This resulted in the final spectra for the components.

The assumption of a smoothly varying component angular size allows us to use only a small number of parameters in the final model, resulting in robust estimates of the component spectra even in the size scales significantly smaller than the resolving beam. A more detailed description of our spectral extraction method together with an error analysis is given in Savolainen et al. (A&A, submitted).

3. Component spectra and derived magnetic field densities

The final spectra are presented in Fig. 1. The components within 2 mas from the core show a spectral turnover at our frequency range. We have fitted the spectra of these components with a function describing self-absorbed synchrotron radiation emitted by electrons having a power-law energy distribution in a homogeneous magnetic field. From the fits, values of the turnover frequency, $\nu_{\rm m}$, the maximum flux density reached at the turnover frequency, $S_{\rm m}$, and the optically thin spectral index, α, were derived. These values are given in Table 1

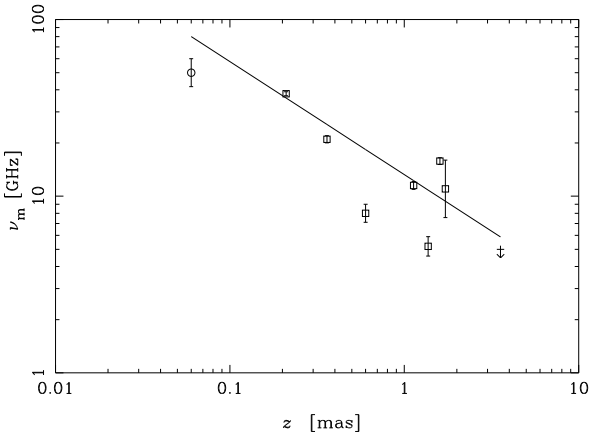

Figure 2. The synchrotron peak frequency as a function of distance along the jet. Since the total radio spectrum of 3C 273 steepens above ~ 60 GHz, the jet cannot stay self-similar beyond the point where $\tau = 1$ surface is at this frequency. The mm-core we observe has $\nu_{\rm m} = 50 \pm 10$ GHz and we do not register any core shift between 43 and 86 GHz images within the accuracy of 0.02 mas. Hence, we conclude that our core component is within 0.06 mas (half the $FWHM$ of the core times a geometrical correction factor of 1.8) from the point where the self-similarity breaks up. We measure the distance z with respect to this point ($z = z_0 + 0.06$ mas). The open circle corresponds to the core, while the downward arrow shows the upper limit of $\nu_{\rm m}$ at $z > 3.5$ mas. The solid line is a power-law fit to the data: $\nu_{\rm m} \propto z^{-0.6\pm0.1}$.

together with the components' distances from the core, z_0, their sizes, a, at $\nu_{\rm m}$, and their Doppler factors, δ, which were measured in Paper I.[1]

In Fig. 2 we have plotted $\nu_{\rm m}$ as a function of distance along the jet, z, in a logarithmic scale. The peak frequency seems to decrease rather steadily as a function of z. A simple power-law fit to the peak frequencies gives $\nu_{\rm m} \propto z^{-0.6\pm0.1}$, at least within 2 mas from the core. This confirms the compound nature of 3C 273's flat radio spectrum: components become self-absorbed at progressively lower frequencies as they move out along the jet creating an apparently flat radio spectrum up to $60 - 90$ GHz (see Fig. 8 in Courvoisier 1998).

Adopting the standard synchrotron theory and assuming that emission features are uniform and spherical, we have used the observed component spectra – together with the measured sizes and Doppler factors – to estimate the magnetic field density, B, the electron energy distribution normalization factor, N_0, and the relativistic electron energy density, $U_{\rm re}$, of the components in Table 1. The formulae are given in Marscher (1987). Since we have *measured* $\nu_{\rm m}$, $S_{\rm m}$, δ and a, we can calculate B and N_0 separately without having to assume equipartition conditions. The component size inserted in the formulae is 1.8 times the $FWHM$ of the Gaussian component (Marscher 1987). Since δ was determined only for components C2, B2, B3 and B4 in Paper I, we have used an average

[1]There was an error in the Doppler factor reported for component B2 in Paper I. Table 1 contains the correct value. This value of Doppler factor, together with $\beta_{\rm app} = 6.5 \pm 0.6$, yields a Lorentz factor of 6.6 ± 1.4 and a viewing angle of $8.1 \pm 3.0^\circ$ for B2.

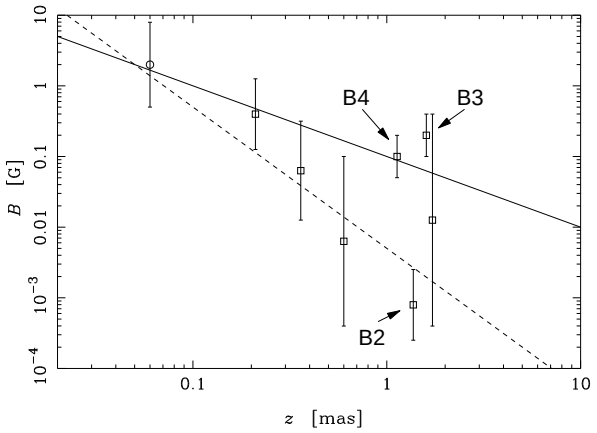

Figure 3. Magnetic field density of the jet components as a function of distance along the jet. The open circle corresponds to the core component. The solid and dashed lines show examples of a power-law dependence $B \propto z^b$ with $b = -1$ and $b = -2$, respectively.

value $\langle\delta\rangle = 5.6$ for the rest of the components. The very strong non-linear dependence of B, N_0, and $U_{\rm re}$ on the observed quantities makes a linear approximation of the error propagation invalid, and we have employed a Monte Carlo approach to calculate the uncertainties. The results are listed in Table 2.

4. Discussion

Fig. 3 shows B as a function of z, in a logarithmic scale. The core has magnetic field density of an order of 1 Gauss, which is compatible with the values derived from infrared and optical variability (Courvoisier et al. 1988). Generally, the magnetic field becomes weaker as we move out along the jet. However, there is a large discrepancy in B between components B2 and B3, both having about the same distance from the core. Component B2, which is located ≈ 0.6 mas north of B3, has two orders of magnitude smaller B than component B3 (or B4). The kinematic analysis presented in Paper I already showed that there is a significant velocity gradient across the jet width at the same location: the northern component B2 has a bulk Lorentz factor $\Gamma = 6.6 \pm 1.4$, while the southern components B3 and B4 have $\Gamma = 17 \pm 7$ and $\Gamma = 18 \pm 8$, respectively. The magnetic field and velocity gradients across the jet width are thus coincident: the slower northern component B2 has significantly smaller B than the faster southern components B3 and B4. Are we seeing a spine/sheath structure in 3C 273 (with B3 and B4 corresponding to a fast spine and B2 to a slower layer), where the magnetic field density decreases from the high jet-axis value to the lower value in the sheath? An argument against this interpretation is the absence of emission from the jet layer south of the spine. However, if the magnetic field in the layer has a large enough helical component, emission asymmetries can arise (Roca-Sogorb et al. in these proceedings).

An average value of $U_{\rm re}$ within 2 mas from the core is about $10^{-4}\,{\rm erg\,cm^{-3}}$. The core has significantly more energy in the magnetic field than in the radiating

Table 2. Physical parameters of the emission regions

Comp.	z_0 (mas)	$\log_{10}(B)$ (Gauss)	$\log_{10}(N_0)$ ($\mathrm{erg}^{-2\alpha}$ cm^{-3})	$\log_{10}(U_{\mathrm{re}})$ ($\mathrm{erg\ cm}^{-3}$)	$\log_{10}(U_{\mathrm{B}}/U_{\mathrm{re}})$
Core	0.00	$+0.3 \pm 0.6$	-6.9 ± 1.8	-5.0 ± 1.2	$+4.2 \pm 1.6$
C2	0.15	-0.4 ± 0.5	-4.2 ± 1.2	-3.8 ± 1.3	$+1.7 \pm 1.6$
C1	0.30	-1.2 ± 0.7	-6.4 ± 1.9	-3.7 ± 1.6	-0.1 ± 2.1
B5	0.54	-2.2 ± 1.2	-7.6 ± 3.6	-3.7 ± 2.7	-2.1 ± 3.6
B4	1.07	-1.0 ± 0.3	-6.1 ± 1.1	-5.2 ± 1.1	$+1.9 \pm 1.3$
B2	1.31	-3.1 ± 0.5	-3.5 ± 1.4	-2.1 ± 1.3	-5.5 ± 1.6
B3	1.54	-0.7 ± 0.3	-7.2 ± 1.2	-5.0 ± 1.0	$+2.3 \pm 1.2$
B1	1.66	-1.9 ± 1.5	-2.2 ± 2.3	-2.2 ± 2.6	-3.0 ± 4.0

particle population, while component B2, on the other hand, is heavily particle dominated. The other components are more or less compatible with a rough equipartition between U_{B} and U_{re}. In addition to magnetic field and electrons, there will be energy stored in cold protons, if the jet is composed of electron-proton plasma. If one cold proton per a relativistic electron is assumed and the jet is required to be rest mass dominated beyond the core instead of being Poynting flux dominated ($U_{\mathrm{p}} > U_{\mathrm{B}}$), components C2, B3 and B4 must have the low energy cut-off of the relativistic electron distribution $\lesssim 10$.

Acknowledgments. This work was partly supported by the Finnish Cultural Foundation (TS), and by the Academy of Finland grants 74886, 210338, and 120516. The VLBA is a facility of the National Radio Astronomy Observatory, operated by Associated Universities, Inc., under cooperative agreement with the U.S. National Science Foundation.

References

Bartel, N., et al. 1984, ApJ, 279, 116
Cotton, W. D., et al. 1980, ApJ, 238, 123
Courvoisier, T. J.-L., et al. 1988, Nature, 335, 330
Courvoisier, T. J.-L. 1998, A&A Rev., 9, 1
Courvoisier, T. J.-L. et al. 2003, A&A, 411, 343
Kovalev, Y. Y., et al. 2005, AJ, 130, 2473
Lobanov, A. P. 1998, A&AS, 132, 261
Marr, J. M., Taylor, G. B., & Crawford III, F. 2001, ApJ, 550, 160
Marscher, A. P., & Broderick, J. J. 1985, ApJ, 290, 735
Marscher, A. P. 1987, in Superluminal radio sources, eds. J. A. Zensus & T. J. Pearson, Cambridge University Press, 280
Marscher, A. P. 1988, ApJ, 334, 552
Roca-Sogorb, M. et al. 2007, in these proceedings
Savolainen, T. 2006, "Multifrequency VLBI Observations of Compact Extragalactic Jets", Annales Universitatis Turkuensis, Ser. A1, Vol. 356
Savolainen, T., et al. 2006, A&A, 446, 71 (Paper I)
Taylor, G. B., & Myers, S. T. 2000, VLBA Scientific Memo 26
Vermeulen, R. C. et al. 2003, A&A, 401, 113
Walker, R. C., et al. 2000, ApJ, 530, 233
Zensus, J. A. 1997, ARA&A, 35, 607